ADVANCED FUNCTIONAL MATERIALS
www.afm-journal.de

Inkjet Printed Negative Supercapacitors: Synthesis of Polyaniline-Based Inks, Doping Agent Effect, and Advanced Electronic Devices Applications

Alessandro Chiolerio, Sergio Bocchini, and Samuele Porro*

Low frequency negative supercapacitors and high frequency negative capacitors are realized developing a polyaniline (PANI) based ink for piezoelectric inkjet printers, water based. PANI is synthesized by oxidation polymerization starting from the aniline dimer, thus avoiding the use of a toxic/mutagen substance such as aniline. In order to work in aqueous phase, the reverse addition of the dimer in the oxidative solution is made. The chlorinated emeraldine salt of PANI is produced and emeraldine base is prepared by dedoping. Two different doped PANI solutions are produced by solubilization of the emeraldine salt in dimethylsulphoxide and addition of respectively trifluorosulfonic acid and camporsulfonic acid, and then used as inks for the fabrication of inkjet-printed tracks of different geometries. The properties of inkjet-printed devices are characterized both in DC and AC regimes, showing very good performances under specific measurement conditions in terms of conductivity, as well as extremely interesting phenomena whose origin is still under debate, such as low frequency negative supercapacitance, high frequency negative capacitance and negative resistance. The realization of the highest negative supercapacitance realized so far, of –2.3 mF @ 30 Hz, corresponding to a specific mass capacity of –799 F g^{-1}, is reported.

1. Introduction

Intrinsically conducting polymers (ICPs) are inherently conducting in nature due to the presence of a conjugated π electron system in their structure. ICPs have a low energy optical transition, low ionization potential, and a high electron affinity.[1] With their discovery in 1960, an attractive subject of research was initiated because of the interesting properties and numerous possibilities of application. It was expected that ICPs would find their output in multidisciplinary areas such as chemical, electrical, electronics, thermoelectric, electroactive applications, membrane, and sensors.[1,2]

Polyaniline (PANI) is an ICP showing relatively low values of conductivity as compared to other ICPs such as doped polyacetylene or polyphenylene, but it has the advantage of high stability and processability.[3] Because of its easy preparation, good environmental stability, interesting redox properties, and outstanding potentiality for application in electronic and optical devices, PANI has become one of the most important conducting polymers and been intensively studied in the last two decades.[4]

PANI can be considered as being derived from alternatively reduced and oxidized forms of the same monomer.[5–7] However, the average oxidation state of the single PANI molecule cannot be varied continuously. Only the completely reduced polymer, the "half-oxidized" polymer and the completely oxidized polymer are stable and at the molecular level all intermediate oxidation states consist of mixtures of the chromophores characteristic of these states.[5,8] The terms leucoemeraldine, emeraldine, and pernigraniline refer to these oxidation states.

In principle, the imine nitrogen atoms can be protonated in whole or in part to give the corresponding salts (**Figure 1**a,b), the degree of protonation of the polymeric base depending on its oxidation state and on the pH of the aqueous acid, because complete protonation of the imine nitrogen atoms in emeraldine base results in the formation of a delocalized polysemiquinone radical cation [6,7,9] (Figure 1c,d) and is accompanied by an increase in conductivity of about ten orders of magnitude. The partly protonated emeraldine salt can be synthesized easily either by the chemical or electrochemical oxidative polymerization of aniline.[5–7] It can be deprotonated by aqueous ammonium hydroxide to give emeraldine base powder (a semiconductor).

Many different acids such as dodecylbenzensulfonic acid (DBSA),[10] poly(4-styrenesulfonic acid) (PSS),[11] trifluoroacetic acid CF_3COOH (TFA),[12] camporsulfuric acid (CSA),[13] and so on were used in order to obtain protonated emeraldine salt.

The ageing of PANI and the loss of electrical properties is usually a consequence of a complex combination of structural changes: deprotonation, loss of conjugation, oxidative processes, crosslinking, and other chemical reactions on PANI chains (chlorination, sulfonation) driven by the doping agent.[15] The doping agent is thus important from the point of view of stability; it could influence deprotonation, which is the main mechanism of ageing and degradation. As an example,

Dr. A. Chiolerio, Dr. S. Bocchini, Dr. S. Porro
Center for Space Human Robotics
Istituto Italiano di Tecnologia
Corso Trento 21, 10129 Torino, Italy
E-mail: alessandro.chiolerio@iit.it

DOI: 10.1002/adfm.201303371

© 2014 WILEY-VCH Verlag GmbH & Co. KGaA, Weinheim

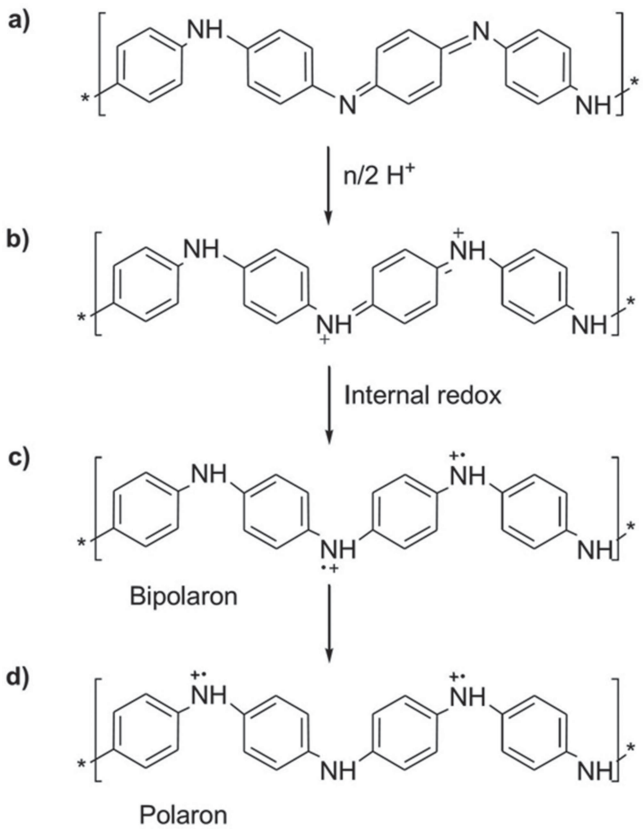

Figure 1. PANI Emeraldine base a) before protonation, b) after 50% protonation, and c) formation of bipolaron and d) polaron forms.[14]

it was reported that the gradual conversion of the PANI salt to base in the case of HCl-doped PANI reduces the conductivity of PANI of about 50% in 500 days.[16] On the other hand, it seems that the relatively fast room temperature loss of conductivity of HCl-doped PANI is a singular case, probably due to the volatility of HCl. The vast majority of doped PANI types results stable below 70 °C.[16] A glass-like transition at about 70 °C has been reported.[17] Generally, it is believed that doped PANI can be used for several years without chemical/structural modifications, independently from the different type of doping agents (except for some very specific cases).

In the available literature different ways to produce PANI have been demonstrated, including chemical, electrochemical, template, enzymatic, plasma, photo, and a number of other unusual methods.[3] Chemical polymerization can be in turn subdivided into heterophase, solution, interfacial, seeding, metathesis, self-assembling, and sonochemical polymerizations.[3] However, aniline is classically chosen as the starting monomer, and the first step of polymerization (**Figure 2**) in acidic solutions is oxidation with the formation of a radical cation (1) and a dimer (2).[18] The radical formed in (1) can be localized either on the nitrogen atom or on the ortho- or para-carbons, which could result in structural heterogeneity of the reaction products. The further oxidation of the aniline dimer (DANI) forms radicals that couple to produce aniline oligomers and thus the PANI (3 and 4).

The chemical polymerization is therefore an autocatalytic process and the limiting step is the formation of the aniline dimer.[19] The direct use of DANI as starting monomer allows avoiding this limiting step obtaining as a plus a more ordered structure, moreover the reaction avoids the use of a toxic/mutagen substance such as aniline. However, the low water solubility of DANI[20] has classically limited its use, thus only a few articles on PANI synthesis starting from DANI were published.[20–23] An alternative method was used by our group by the use of an anionic surfactant such as polystyrene sodium sulfonate to form a stable DANI emulsion in water and thus the use of a classical oxidant such as ammonium persulfate.[24] However, this method has the drawback that the counterion in the doped PANI should be the emulsioning agent. This problem can be solved by reserve addition of DANI into the oxidant solution. In fact, by direct addition of DANI in the solution of ammonium persulfate the pernignaline was obtained and thus, once the oxidant was exhausted, exceeded DANI was oxidized by the pernigraniline, allowing formation of the emeraldine form as already demonstrated previously.[25] This method allows having other counterions in the final compounds, such as the classical chlorine anion or other counterions obtained by dedoping and doping. In this work, the synthesis of a printable PANI-based ink by DANI polymerization using reverse addition is presented. The obtained PANI emeraldine salt doped with chlorine anions was dedoped and thus used to prepare inks of PANI doped with CSA and trifluoromethylsulfonate acid (TFMS) in order to increase PANI electrical properties. The physical and chemical properties of the developed polymer, its printing on flexible polymeric substrates and the electrical properties of printed tracks were studied. In particular,

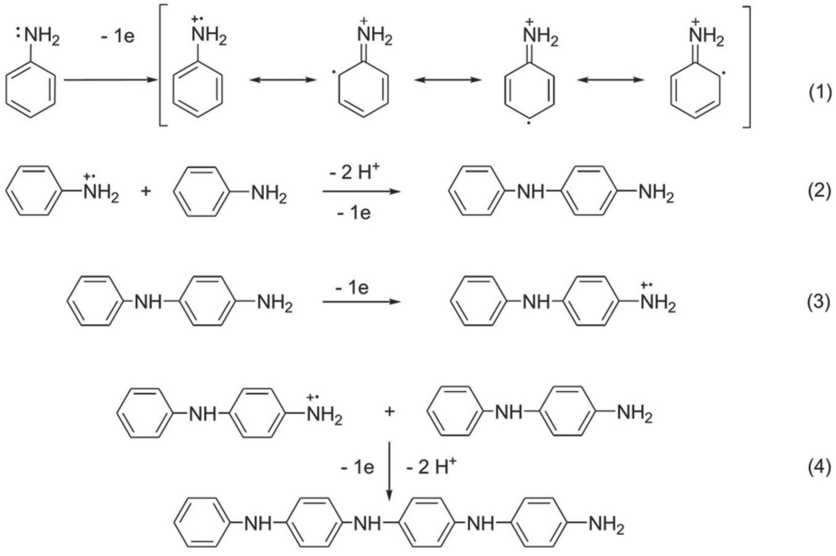

Figure 2. Mechanism of PANI synthesis starting from aniline.

© 2014 WILEY-VCH Verlag GmbH & Co. KGaA, Weinheim

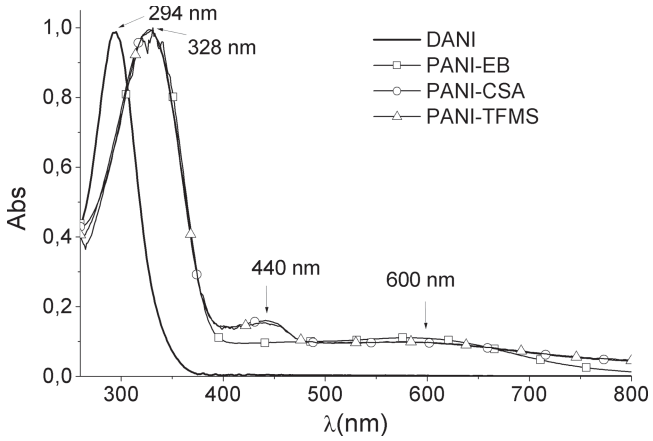

Figure 3. UV–vis spectra of DANI (N-phenyl-1,4-phenylendiamine), PANI-EB (Polyaniline emeraldine base), PANI-CSA (Polyaniline emeraldine salt doped with camphorsulfuric acid) and PANI-TFMS (Polyaniline emeraldine salt doped with trifluorometansulfonic acid). DMSO solvent was subtracted and results were normalised to the π–π* transition peak for all the solutions.

we focused on DC and AC analyses up to 2 MHz. This work opens new interesting possibilities of actively controlling the electronic properties of devices based on PANI ink realized by means of inkjet printing, whose versatility is well known in realizing additively manufactured circuits.[26–30]

2. Results and Discussion

2.1. UV-VIS

In **Figure 3** the UV–vis spectra of DANI, PANI-EB, PANI-CSA and PANI-TFMS doped in DMSO solution are reported. In order to have comparable results, the DMSO spectrum was subtracted for all the solutions and the results were normalized to have maximum absorbance equal to 1. In this solvent, as for the majority of available solvents, PANI adopts compact-coil conformation with the expected bands both for the emeraldine base and the emeraldine salt.[31] The DANI shows a single peak at 294 nm due to the π–π* transition as expected for an aromatic molecule. Because of higher conjugation, this band shifts to higher λ in the case of the polymer. This peak is perfectly superimposable for the emeraldine base of PANI and the doped forms. In the case of PANI doped with CSA and TFMS, a band with a maximum at 440 nm appears, ascribed to the polaron–π* transition that gives a green color to the solution. This band is independent from the acid used, demonstrating a complete protonation in both cases. Finally, the emeraldine base shows a band at ≈600 nm arising from n–π* transition.

2.2. Infrared Analysis

The FTIR spectrum of PANI-EB (**Figure 4**) shows main absorbance of PANI assessing its formation. The strong band with maximum at 3250 cm^{-1} has often been attributed to

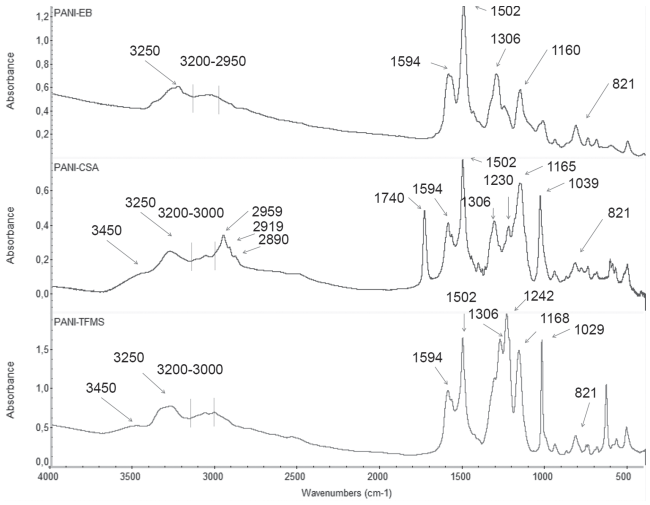

Figure 4. FTIR spectra of PANI-EB, PANI-CSA, and PANI-TFMS.

different types of intra- and inter-molecular hydrogen-bonded $\nu_{N\text{-}H}$ stretching vibrations of secondary amines.[32] The 3100–2950 cm^{-1} zone shows the ν_{CH} of aromatic rings.[33] The band at 1594 cm^{-1} is attributed to C=N stretching of quinoid diimine unit (the oxidised form of PANI). C–C aromatic ring stretching of the benzenoid diamine unit (the reduced form of PANI) appears at 1502 cm^{-1}.[34,35] The 1306 cm^{-1} is attributed to the C–N stretching of aromatic amines.[35] The 1160 cm^{-1} peak refers to the stretching of quinoid ring.[35] The 821 cm^{-1} peak is the absorbance of the out of plane bending for para-disubstituted benzene[36] confirming the formation of the right polymer configuration.

The addition of CSA partially changes the infrared spectrum. All the absorbance features described above were still present, with the addition of the bands due to CSA anion. The 3450 cm^{-1} is due to the ν_{NH} formed in the emeraldine salt.[37] The 2959, 2919 and 2850 cm^{-1} bands are the ν_{CH} of the CSA aliphatic part.[36] The 1740 cm^{-1} peak is the $\nu_{C=O}$ of the ketonic group of CSA,[36] while the 1230 and 1039 cm^{-1} are respectively the asymmetrical and symmetrical ν_{SO3-} of the camphor sulfonic salt.[38] The TFMS salt of PANI has absorbance similar to the CSA salt, the main differences being the absorbance at 1242 and 1029 cm^{-1} (respectively the asymmetrical and symmetrical ν_{SO3-}).[39]

2.3. Thermal Gravimetric Analyses

The results from TGA in nitrogen and air for the starting dimer (DANI) and PANI-EB are shown in **Figure 5**. The dimer shows one main degradation step both in nitrogen and air atmosphere with maximum degradation rate respectively at 273 °C and 263 °C. The boiling point of this compound is about 360 °C (database source)[40] thus this weight loss is probably due to the thermal decomposition of the molecule with formation of volatile fragments. There are not enough data to define the decomposition mechanism, however, taking into account the mechanism of polyaniline polymerization, a dismutation of the dimer with fragmentation to aniline and volatile diazide

© 2014 WILEY-VCH Verlag GmbH & Co. KGaA, Weinheim

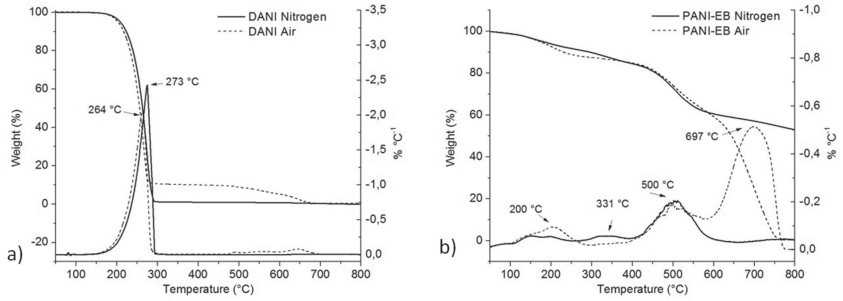

Figure 5. Thermal degradation of a) DANI and b) PANI-EB at 10 °C min^{-1}, respectively in nitrogen (continuous lines) and air (dotted lines). Derivative curves are also reported.

compounds can be supposed. This mechanism is supported from the anticipation of the reaction in oxygen atmosphere: in fact, oxygen is a well known initiator of radical reactions by formation of radicals by hydrogen abstraction. The TGA of PANI-EB in nitrogen and air are completely different from the starting monomer (Figure 5b). Two major stages of weight losses for PANI-EB in nitrogen have been reported.[41]

The first at lower temperature results from moisture evaporation and perhaps outgassing of unknown small molecules. The second at higher temperature indicates a structural decomposition of the polymer. Because of the drying step during preparation, the first degradation step is very small and it is a continuous weight loss from 100 °C to 400 °C with a maximum at about 331 °C. In our case, the low molecular weight and the formation of by-products from the polymerization reaction of PANI are probably responsible for this weight loss. The main degradation step is at about 500 °C, probably due to formation of carbon char with the elimination of nitrogen and hydrogen, for example, by production of ammonia. The TGA of PANI-EB in air is quite similar. In this case the first degradation step is anticipated at 200 °C because of the oxidizing atmosphere. The second step is similar, demonstrating that the nitrogen elimination is consisting with the results. In this case, a final step of weight loss due to carbon char oxidation at about 700 °C is present as expected in oxidizing atmosphere.

2.4. Morphology of Inkjet-Printed Tracks

Imaging by optical microscopy was performed on the inkjet-printed tracks in order to evaluate the homogeneity of printing and understand if doped PANI tends to form an emulsion and thus retaining a particle shape or dissolve as occurs in a solution. The analysis demonstrated a good printability of the PANI-based inks: the tracks resulted homogeneously deposited without evidence of irregularities. The printed material presented microstructuring (**Figure 6**), moreover, at the edges of the printed tracks, a coffee-stain effect is visible (more or less pronounced depending on sample), probably due to the fact that the evaporation rate of the used solvent (DMSO) is slower than crystallization of the solid phase.

As demonstrated by electrical characterization, the presence of these features does not hamper the electron percolation nor influence the overall properties of the devices. Cross-sectional views of the printed tracks obtained by profilometry are shown in **Figure 7**, where PANI-CSA and PANI-TFMS are compared (both 1 and 3 passes). Each profile shown in Figure 7 is the numerical average of ten profile acquisitions performed in direction orthogonal to each inkjet printed track along their full length of 2 cm, the error bars representing the standard deviation from the average. Substrate bending–bowing was compensated by subtracting a polynomial fit, while other positioning errors–offsets were compensated by a numerical alignment routine based on the computation of the first derivative of the profile.

Although the nominal width is 100 μm, the effective track width may vary considerably from the nominal value, being 2.5 times larger in the case of PANI-CSA (both 1 and 3 passes) and up to 4 times larger for PANI-TFMS (3 passes). The surface roughness of the printed tracks is quite high for PANI-CSA as indicated by the error bars, which in the case of single pass extend up to 50% of the mean track height, whilst in the case of 3 passes are close to 20%. For PANI-TFMS, surface roughness

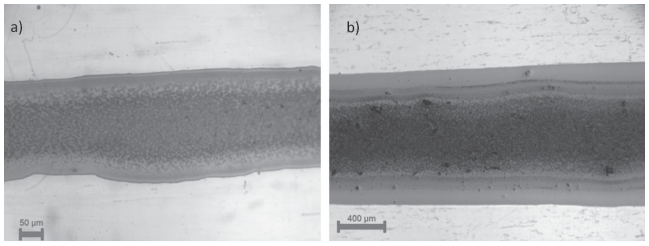

Figure 6. Optical microscopy images of a portion of a) PANI-CSA and b) PANI-TFMS printed tracks showing coffee-stain effect.

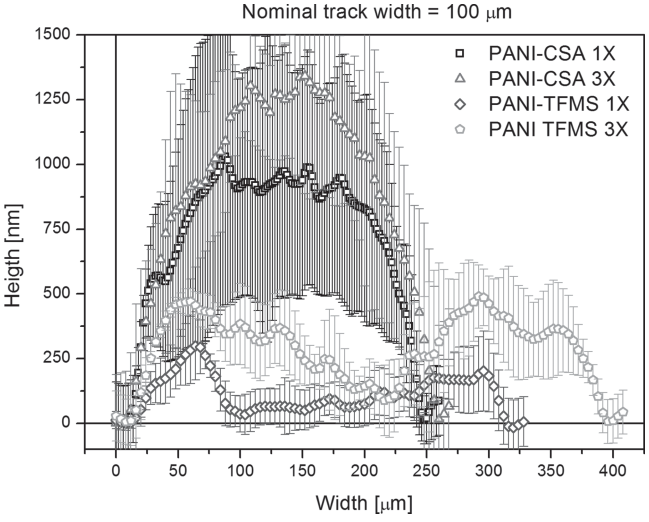

Figure 7. Average cross-sectional profile as acquired by profilometry of PANI-CSA and PANI-TFMS printed tracks (1 and 3 passes). For clarity, only one point every three measured is shown.

© 2014 WILEY-VCH Verlag GmbH & Co. KGaA, Weinheim

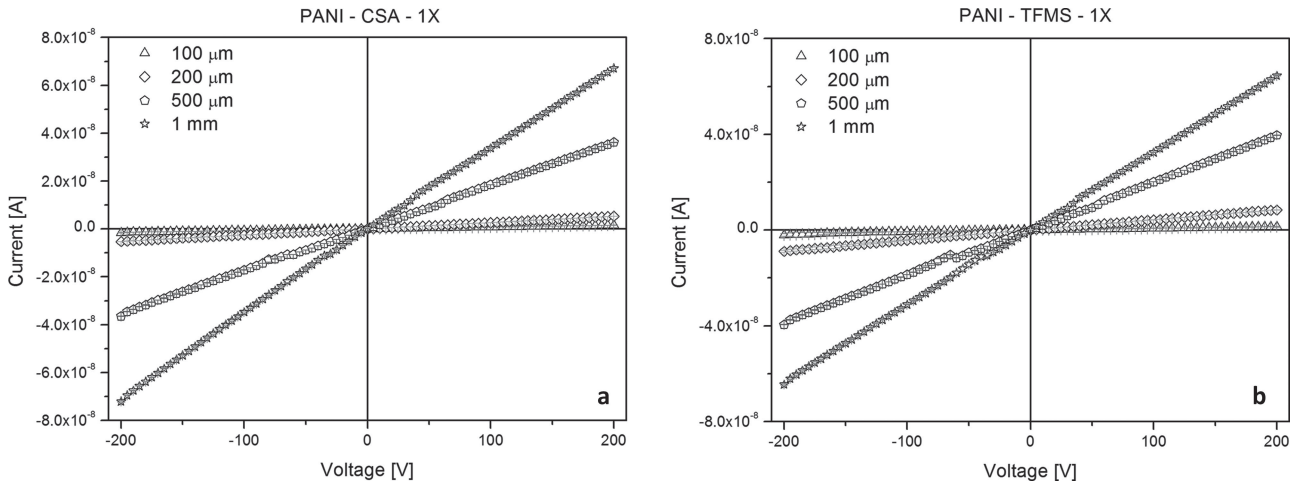

Figure 8. *I–V* curves of inkjet-printed a) PANI-CSA tracks and b) PANI-TFMS tracks. The plots refer to a single pass.

is close to 35% and seems independent from the number of passes.

The typical profile is regular for PANI-CSA, whilst a coffee-stain effect is revealed for PANI-TFMS. This effect can be explained by the occurrence of complex solvent evaporation dynamics due to accumulation of deposited material, which is more likely at the edges.

The differences in the track profile/width can also be attributed to the different hydrophobicity of the materials, in the case of CSA the counterion is more hydrophobic than TFMS, which is polar and thus hydrophilic. Taking into account the polar nature of the polyamide substrate it is natural that the PANI-TFMS ink tends to form larger tracks.

2.5. Electrical Properties

2.5.1. DC Analyses

In **Figure 8**a, the *I–V* curves of the inkjet-printed PANI-CSA are reported, related to a single pass pattern. Track widths of 100, 200, 500 μm, and 1 mm are compared. It is clear that the transport regime is not based on diffusion, since the highest currents are always sustained by the widest lines. However, increasing the number of passes (Figure S1, Supporting Information) produces a negative effect on the overall performance of the material, causing a four-fold reduction of the current density through the printed tracks, as will be commented in the following.

In Figure 8b, the *I–V* curves of the inkjet-printed PANI-TFMS are reported, related to a single pass pattern. Once again the highest currents are sustained by the widest lines, but in this case increasing the number of passes produces a dramatic increase in track conductance, by almost one order of magnitude (Figures S2,S3, Supporting Information). In particular, the effect produced by increasing the number of passes may be seen in the phase-plot shown in **Figure 9**, where the measured resistivities of all tracks of the two compositions are compared, both at 1 and 3 passes. Remarkably, the experimental errors are very low (error bars collapsed) with the only exception of the sample PANI-TFMS 3 passes 1 mm in width, whose quite high error (10%) may be explained in terms of an anomalous geometry reproduction (image not shown). Thus, neglecting this single point, it is possible to observe that the resistivities of all 3 passes tracks are almost independent on the track width (as logical), confined in the same order of magnitude. On the contrary, the single pass track resistivities are more dependent on the nominal width, since their geometry may include local restrictions limiting the maximum current, which disappear in thicker tracks. The ultimate resistivity in the best experimental case (PANI-TFMS, 3 passes, 200 μm track width) was calculated to be 990 Ω cm. Please note that the resistivity values shown in Figure 9 are based on real measurements of track thickness, according to average cross-sectional profiles data (Figure 7).

2.5.2. AC Analyses

The characterization of electrical properties was completed by acquiring a full set of AC measurements in the range

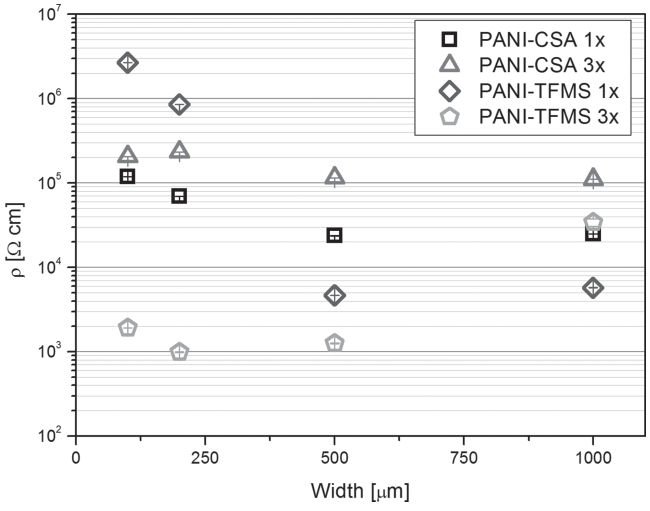

Figure 9. Resistivity versus track width for PANI-CSA and PANI-TFMS transmission lines printed at different conditions: single and triple pass.

© 2014 WILEY-VCH Verlag GmbH & Co. KGaA, Weinheim

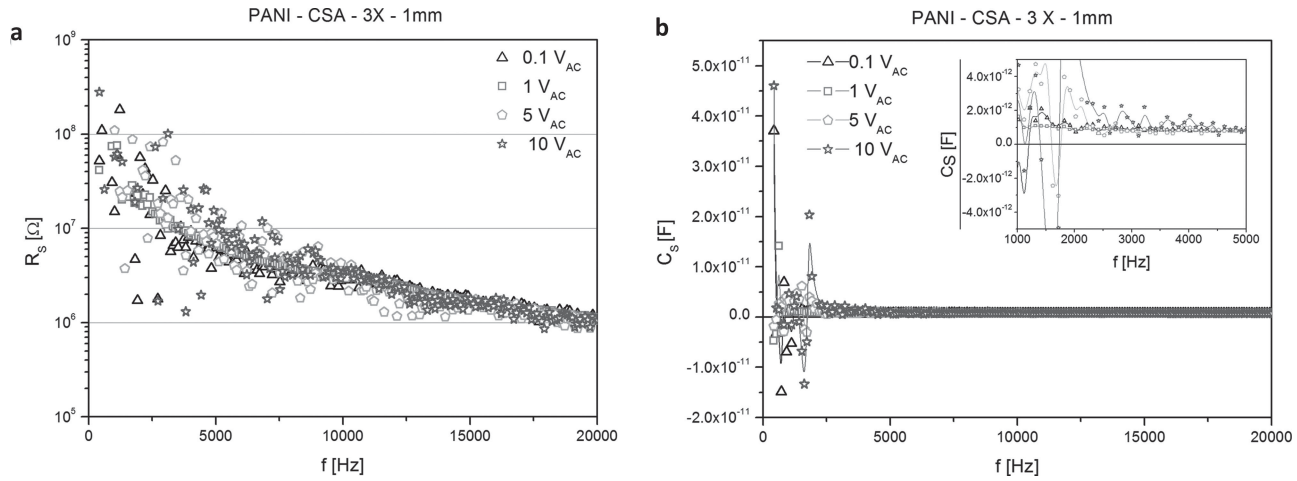

Figure 10. Series resistance of the widest/thickest track of PANI–CSA (1 mm in width, triple pass) as a function of a) signal amplitude and b) series capacitance, including a magnification of the 1 to 5 kHz region shown in the inset.

20 Hz–2 MHz. Starting from PANI–CSA devices, the presence of a negative capacitance was observed, particularly in the low frequency range. The series resistance (**Figure 10**a) and capacitance (Figure 10b) were calculated as a function of the signal amplitude, varied between 10 mV and 10 V, for a 1 mm-wide track (triple pass). In particular, Figure 10b shows a dispersion of experimental points revealing a small negative capacitance (absolute value around 15 pF) for each curve.

A low frequency negative supercapacitance was found in the case of PANI–TFMS tracks. Starting from a small signal, having amplitude of 1 V, resistance fluctuations around zero in the low frequency regime and a negative capacitance in the nF range (hence two orders of magnitude higher with respect to PANI–CSA) were found (Figures S4,S5, Supporting Information). By increasing the signal amplitude to 5 V (Figure S6,S7, Supporting Information), a more pronounced negative capacitance was observed in the same frequency range, reaching a value around some units of μF. It is remarkable that the series resistance curves are such that an algebraic average performed on the experimental curves would produce a value close to zero, while each measurement is such that the resistance fluctuates between very small values of some hundreds of Ohms. Finally, increasing the signal amplitude up to 10 V (**Figure 11**a,b), huge negative capacitances up to some mF were observed at very low frequencies, meaning that this material could be very interestingly exploited as negative supercapacitor, for devices running at commercial grid frequencies (50, 60 Hz). Once again, the resistance state oscillates between negative and positive values after experiencing a high conductivity state. A variation in the number of passes is reflected in the absolute maximum value of negative capacitance reached: for example tracks at one pass result in negative capacitances in the order of nF; furthermore both resistance and reactance are reduced, and also the typical low frequency response shows a slight difference. Figure S8 (Supporting Information) shows in logarithmic scale a comparison between the response of a 1-pass track and a 3-passes track.

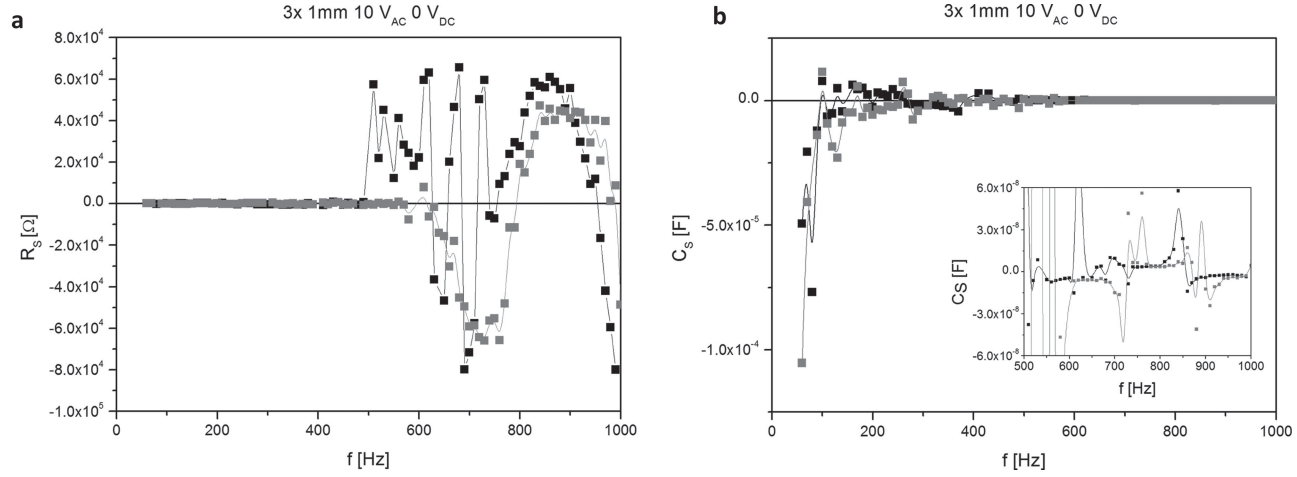

Figure 11. Series resistance of a PANI–TFMS track (1 mm in width, triple pass) measured in two subsequent experiments in the low frequency range for a) signal amplitude of 10 V and b) series capacitance, including a magnification of the 500 to 1000 Hz region shown in the inset.

© 2014 WILEY-VCH Verlag GmbH & Co. KGaA, Weinheim

3. Discussion

The production of polyaniline from DANI was already performed in literature however all the methods developed need longer times because of the low solubility of DANI in water[23] or they are effective for specific synthesis such as functionalization.[21] From the analyses of the PANI-EB obtained by the reverse addiction of DANI to the oxidant solution it was demonstrated that the rapid production of PANI with a scalable method was feasible. The structure and properties of the resulted PANI were confirmed by Fourier transform infrared, UV–vis and thermal gravimetric analyses.

The optimized rheological properties of both PANI-CSA and PANI-TFMS inks resulted in an excellent jettability of the material and very good geometry realization, which represent the first requirement for the realization of advanced electronic devices. The second requirement is an optimal cross-sectional profile, which could be obtained for PANI-CSA according to our cross-sectional analyses, while PANI-TFMS suffers from coffee-staining and material accumulation in correspondence of the track edges, however these effects can be avoided by the optimization of the printing process or by the addition of another solvent.

Inkjet printed devices showed unexpected behavior. Despite their high conductivity, in the range between 10^5 and less than 10^3 Ω cm, we have seen negative supercapacitance and anomalous negative capacitance, at frequencies much higher than those naturally arising from complex carrier mobility. For what concerns DC electrical properties, we have seen that PANI-CSA results in almost constant and uniform resistivity values both for a single pass and for multiple passes, probably because of the optimized cross-sectional profiles and optimal geometry reproduction. PANI-TFMS produces uniform and constant resistivities only in the case of multiple pass, probably because of coffee-staining and poor geometry reproduction. Nevertheless, geometry reproduction problems may be solved by multiple pass printing, allowing to feature the lowest measured resistivity of 990 Ω cm.

Moving to the AC range, we may point out that the heterogeneous system under study, formed by a dispersion of crystalline PANI domains in an amorphous PANI matrix, where the mobility of doping counterions is higher in the latter environment, because of the higher free volume, may be characterized in two different regimes. Where the measurement frequency is such that the ion mobility is able to follow the signal (below 1 kHz), we could identify interesting phenomena such as negative resistance/capacitance and supercapacitance, resulting from the counterion displacement induced by the measurement signal. Providing that the frequency is well above the characteristic diffusion time scale of counterions (above 1 kHz), we could measure conventional behavior comprising small positive parasitic capacitance and a decreasing resistive component. But even in the range below 1 kHz, it is possible to evidence two different phenomena. The first phenomenon involves charged carrier trapping, which cannot respond to the AC driving voltage and result, when the transit time is comparable to the retention time, in an opposite phase.[42] This occurs at frequencies comprised between 20 (which is our instrumental lower bound) and 300 Hz, and the minimum negative supercapacitance measured was –2.3 mF @ 30 Hz for PANI-TFMS 1 mm-track realized in 3 passes, sampled at 5 V_{AC}. This value represents the biggest negative capacitance realized so far; considering the surface/mass of the device, we obtained a specific negative capacity of –3.8 mF cm^{-2} (surface) –799 F g^{-1} (gravity). The second phenomenon is such that negative capacitances arise in the polymer even around 1 kHz, being far too above the typical retention times of trapped charges in our system.

We may deduce that interesting practical applications such as negative capacitors/negative supercapacitors could be found in the low frequency range, for those devices working at nominal grid conditions (50–60 Hz) and up to short waves radio frequencies. Negative capacitors are extremely interesting objects which could fully compensate ubiquitous losses induced by parasitic capacitances in commercial devices.

4. Conclusions

We reported on the fabrication of inkjet printed all-polymer flexible devices featuring interesting properties, such as low frequency negative supercapacitance, high frequency negative capacitance, negative resistance, and high DC conductance. Furthermore, a new synthesis for PANI starting from DANI was developed, and it was demonstrated that the facile and fast production of PANI soluble in organic solvents such as DMSO can be obtained by the reverse addition of a organic solvent solution of DANI in the oxidant solution. The synthesis can be performed without the use of toxic/mutagenic reagents such as aniline and thus in a safer environment. By a classical action of de-doping and doping, it is thus possible to obtain PANI with the preferred counterions on the basis of the requirements such as in our case, where two different inks were prepared with excellent jettability and very good geometry realization.

The produced inks have almost constant and uniform resistivity values; moreover, they show interesting phenomena such as negative resistance/capacitance and supercapacitance, resulting from the counterion displacement induced by the measurement signal. Practical applications, such as negative capacitors/negative supercapacitors, could be found in the low frequency range, for those devices working at nominal grid conditions (50–60 Hz) and up to short waves radio frequencies.

5. Experimental Section

Materials: N-phenyl-1,4-phenylendiamine 98%, that is the aniline dimer (DANI), (1S)-(+)-10-Camphorsulfonic acid (CSA) 98%, trifluoromethanesulfonic acid (TFMS), ammonium persulfate (APS) 98%, hydrochloric acid 37 wt%, ammonium hydroxide 28–30 wt% dimethylsulfoxide (DMSO) 99.9% were purchased from Aldrich and used as received.

PANI Synthesis: 40 mL of a solution of DANI (4 mmol, 0.9212 g) in DMSO was added drop by drop to 360 mL of a solution of APS (6 mmol, 1.369 g) in HCl 0.1 M. During the addition the solution first turned violet, then blue and eventually dark green demonstrating the formation of Cl-doped PANI. After 3 h, the product was firstly separated by filtration and then washed with both double distilled water and ethanol. The product was a green powder. In order to obtain dedoped PANI, the green powder was added to 400 mL of a solution of ammonium hydroxide 0.1 M. After 24 h the solution was filtered and the PANI in the emeraldine

© 2014 WILEY-VCH Verlag GmbH & Co. KGaA, Weinheim

base form was obtained (PANI-EB). Finally, PANI-EB was washed with double distilled water and dried at 60 °C until constant weight.

PANI Inkjet Printing Process: The samples of doped PANI were prepared by dissolving PANI-EB in DMSO, subsequent addition of CSA (PANI-CSA) or TFMS (PANI-TFMS) (0.5 mol every 1 mol of nitrogen atom in PANI) and thus diluted in DMSO at the concentration of 5.0 wt% with respect to the doped formula.

The solutions were stable for a limited time before jellying (normally 1–2 d), thus they needed a one-hour ultrasonication step just before printing, in order to warrant dispersion of the polymer into the solvent. The solutions were then inserted into a 3 mL reservoir and loaded to the inkjet printing system (JETLAB 4-XL from Microfab, US). The system is equipped with independent heaters for the printing nozzle and the substrate, with the possibility of printing a maximum size of 21 cm × 26 cm. Printing tests were achieved through piezoelectric nozzles made in quartz, with diameter of 80 μm, with a vibration frequency set to 250 Hz for PANI-CSA and 500 Hz for PANI-TFMS. The three-axis movement and the values of voltage and wave form that command the piezoelectric nozzle were computer controlled, and the dimension and speed of ink drops were controlled by a horizontal camera located onto the x-y stage for direct drop observation. Jetting parameters were set as follows, using an asymmetrical pulse: first rise time 12 μs, dwell time 15 μs, fall time 5 μs, echo time 20 μs, second rise time 2 μs, idle voltage 0 V, dwell voltage 35 V, echo voltage –13 V. The nozzle and substrate holder were heated to a temperature of 30 °C in order to obtain the correct value of ink viscosity suitable for printing. All samples were printed onto commercial polyimide sheets (poly-oxydiphenylene-pyromellitimide) and let dry in air. Using the described printing setup, ink drops with diameter of ≈100 μm were normally obtained. Consequently, the script used for test tracks printing was set to achieve a drop spacing of 100 μm to achieve complete coverage of the substrate. For the electrical characterization, standard arrays of tracks having widths of 100, 200, 500 μm, and 1 mm were used, depositing patterns at single, double and triple passes.

UV-Vis Characterization: Absorption spectra were recorded in the wavelength range of 190–800 nm at room temperature using a Cary 5000 UV–vis-NIR spectrometer using DMSO solutions.

Fourier Transformed Infrared Spectroscopy (FT-IR): FT-IR transmittance spectra were collected on a Nicolet 5700 FTIR Spectrometer (ThermoFisher). The samples were prepared via casting on Si wafer from DMSO. 64 scans were signal-averaged at a resolution of 2 cm^{-1} from 4000 to 400 cm^{-1}.

Thermal Gravimetric Analyses (TGA): TGA was carried out on about 10 mg samples using a TG 209 F1 Libra (NETZSCH GmbH), at 10 °C min^{-1} heating rate, from 25 °C to 800 °C under nitrogen or air flow (60 cm^3 min^{-1}). The reported thermal degradation temperatures were the temperatures of maximum weight loss rate (T_{max}). The weight residue percentage (wt_{res}) was taken at 800 °C. Experimental error was estimated to be by typically less than 0.05 mg (approximately ± 0.5%).

Dimensional Analysis of Printed Tracks: The thickness and width of the printed tracks was measured by profilometer (Tencor PLA 10) with a scanning speed adjusted between 50–100 m s^{-1}, sampling rate 50–100 Hz, scan length 1–3 mm and force applied to the tip 0.5–1 mg. The length of the printed tracks was measured by optical microscopy. The measured values were used in the calculation of resistivity from I–V electrical measurements. In particular, each track was profiled in five different points, successively averaged and integrated in order to extrapolate the cross-sectional area.

Electrical Properties: Electrical properties were tested on printed tracks and on a self-standing film obtained by deposition of the same solution used for inkjet printing on a Teflon film and dried under vacuum at 60 °C until constant weight. Standard 2-point micro-contact setup[29] was used at room temperature, both in DC and in AC regime, up to 2 MHz, using a Keithley 2635A multimeter (DC) and an Agilent E4980A precision LCR meter (20 Hz up to 2 MHz).

Received: September 30, 2013
Revised: December 25, 2013
Published online: February 12, 2014

[1] J. Unsworth, B. A. Lunn, P. C. Innis, Z. Jin, A. Kaynak, N. G. Booth, *J. Intel. Mater. Syst. Str.* **1992**, *3*, 380.
[2] a) K. F. Schoch, *IEEE Electron. Insul. Mater.* **1994**, *10*, 29; b) M. Angelopoulos, *IBM J. Res. Dev.* **2001**, *45*, 57; c) N. Gospodinova, L. Terlemezyan, *Prog. Polym. Sci.* **1998**, *23*, 1443.
[3] S. Bhadra, K. Dipak, N. K. Singha, J. Lee, *Prog. Polym. Sci.* **2009**,*34*, 783.
[4] a) A. Ray, G. E. Asturias, D. L. Kershner, A. F. Richter, A. G. MacDiarmid, A. J. Epstein, *Synth. Met.* **1989**, *29*, 141; b) A. G. MacDiarmid, *Angew. Chem. Int. Ed.* **2001**, *40*, 2581; c) E. Kang, K. G. Neoh, K. L. Tan, *Prog. Polym. Sci.* **1998**, *23*, 277.
[5] A. G. MacDiarmid, A. J. Epstein, *Faraday Discuss.* **1989**, *88*, 317.
[6] J. C. Chiang, A. G. MacDiarmid, *Synth. Met.* **1986**, *13*, 193.
[7] A. G. Macdiarmid, J. C. Chiang, A. F. Richter, A. J. Epstein, *Synth. Met.* **1987**, *18*, 285.
[8] a) A. G. MacDiarmid, A. J. Epstein, in "Science and Applications of Conducting Polymers" (Eds.: W. R. Salaneck, D. T. Clark, E. J. Samuelsen), Adam Hilger, Bristol **1990**, p. 117; b) F. L. Lu, F. Wudl, M. Nowak, A. J. Heeger, *J. Am. Chem. Soc.* **1986**, *108*, 8311; c) Y. Sun, A. G. MacDiarmid, A. J. Epstein, *J. Chem. Soc., Chem. Commun.* **1990**, *7*, 529.
[9] A. G. MacDiarmid, J. C. Chiang, A. F. Richter, N. L. D. Somasiri, A. J. Epstein, in Conducting Polymers (Ed.: L. Alcacér), Reidel, Dordrecht **1987**, p. 105.
[10] D. Han, Y. Chu, L. Yang, Y. Liu, Z. Lv, *Colloids Surf., A* **2005**, *259*, 179.
[11] J. Jang, J. Ha, K. Kim, *Thin Solid Films* **2008**, *516*, 3152.
[12] J. Nizioł, E. Gondek, K. J. Plucinski, *J. Mater. Sci.: Mater. Electron.* **2012**, *23*, 2194.
[13] a) Y. Cao, P. Smith, A. J. Heeger, *Synth. Met.* **1992**, *48*, 91; b) Y. Cao, P. Smith, *Polymer* **1993**, *34*, 3139; c) G. Gustafsson, Y. Cao, G. M. Treacy, F. Klavetter, N. Colaneri, A. J. Heeger, *Nature* **1992**, *357*, 477.
[14] S. Bhadra, K. Dipak, N. K. Singha, J. Lee, *Prog. Polym. Sci.* **2009**, *34*, 783.
[15] P. Rannou, M. Nechtschein, *J. Chim. Phys. Phys.-Chim. Biol.* **1997**, *95*, 1410.
[16] V. Jousseaume, M. Morsli, A. Bonnet, *J. Appl. Phys.* **2000**, *88*, 960.
[17] L. Ding, X. Wang, R. V. Gregory, *Synth. Met.* **2000**, *104*, 73.
[18] a) H. Yang, A. J. Bard, *J. Electroanal. Chem.* **1992**, *339*, 423; b) F. Lux, *Polymer* **1994**, *35*, 2915.
[19] Y. B. Shim, S. M. Park, *Synth. Met.* **1989**, *29*, 169.
[20] G. Shumakovich, A. Streltsov, E. Gorshina, T. Rusinova, V. Kurova, I. Vasil'eva, G. Otrokhov, O. Morozova, A. Yaropolov, *J. Mol. Catal. B: Enzym.* **2011**, *69*, 83.
[21] B. Guo, A. Finne-Wistrand, A. C. Albertsson, *Chem. Mater.* **2011**, *23*, 1254.
[22] I. Rozalska, P. Kulyk, I. Kulszewicz-Bajer, *New J. Chem.* **2004**, *28*, 1235.
[23] M. Grigoras, A. M. Catargiu, F. Tudorache, *J. Appl. Polym. Sci.* **2013**, *127*, 2796.
[24] S. Bocchini, A. Chiolerio, S. Porro, D. Accardo, N. Garino, K. Bejtka, D. Perrone, C. F. Pirri, *J. Mater. Chem. C* **2013**, *1*, 5101.
[25] H. S. Kolla, S. P. Surwade, X. Zhang, A. G. MacDiarmid, S. K. Manohar, *J. Am. Chem. Soc.* **2005**, *127*, 16770.
[26] A. Chiolerio, G. Maccioni, P. Martino, M. Cotto, P. Pandolfi, P. Rivolo, S. Ferrero, L. Scaltrito, *Microelectron. Eng.* **2011**, *88*, 2481.
[27] A. Chiolerio, M. Cotto, P. Pandolfi, P. Martino, V. Camarchia, M. Pirola, G. Ghione, *Microelectron. Eng.* **2012**, *97*, 8.
[28] A. Chiolerio, A. Virga, P. Pandolfi, P. Martino, P. Rivolo, F. Geobaldo, F. Giorgis, *Nanoscale Res. Lett.* **2012**, *7*, 502.
[29] R. Giardi, S. Porro, A. Chiolerio, E. Celasco, M. Sangermano, *J. Mater. Sci.* **2013**, *48*, 1249.
[30] A. Chiolerio, I. Roppolo, M. Sangermano, *RSC Adv.* **2013**, *3*, 3446.
[31] a) Y. Xia, J. M. Wiesinger, A. G. MacDiarmid, A. J. Epstein, *Chem. Mater.* **1995**, *7*, 443; b) X. Jing, Y. Wang, B. Zhang, *J. Appl. Polym. Sci.* **2005**, *98*, 2149; c) A. P. Monkman, in Conjugated polymeric materials (Eds: J. L. Bredas, R. R. Chance) Vol. *182*, Nato ASI Series E: Applied Sciences, Kluwer, Dordrecht, The Netherlands **1990**,

© 2014 WILEY-VCH Verlag GmbH & Co. KGaA, Weinheim

p. 273; d) J. F. Wolf, C. E. Forbes, S. Gould, L. W. Shacklette, *J. Electrochem. Soc.* **1989**, *136*, 2887.
[32] S. Holly, P. Sohár, in: Absorption spectra in the infrared region (theoretical and technical introduction) (Eds: L. Láng, W. H. Prichard) Akadémiai Kiadó, Budapest **1975**, p. 69.
[33] (Eds: D. W. Mayo, F. A. Miller, R. W. Hannah) Course Notes on the Interpretation of Infrared and Raman Spectra, John Wiley & Sons, Inc., Hoboken, NJ, USA **2004.**
[34] J. Tang, X. Jing, B. Wang, F. Wang, *Synth. Met.* **1988**, *24*, 231.
[35] R. Cruz-Silva, J. Romero-García, J. L. Angulo-Sánchez, E. Flores-Loyola, M. H. Farías, F. F. Castillón, J. A. Díaz, *Polymer* **2004**, *45*, 4711.
[36] R. M. Silverstein, F. X. Webster, Spectrometric identification of organic compounds, 6th Ed., John Wiley and Sons, New York **1998**, Ch. 3.
[37] J. Jianming, P. Wei, Y. Shenglin, L. Guang, *Synthetic Met.*, **2005**, *149*, 181.
[38] G. Socrates, G. Socrates, In Infrared and Raman characteristic group frequencies: tables and charts. Wiley, Chichester **2001,** p 221.
[39] D. O. Bennardi, G. P. Romanelli, J. C. Autino, L. R. Pizzio, *Appl. Catal. A* **2007**, *324*, 62.
[40] http://pubchem.ncbi.nlm.nih.gov/summary/summary.cgi?sid=24854480 (last access 29 August 2013) .
[41] C. H. Chen, *J. Appl. Polym. Sci.* **2003**, *89*, 2142.
[42] H. L. Kwok, *Phys. Status Solidi C* **2008**, *5*, 638.

© 2014 WILEY-VCH Verlag GmbH & Co. KGaA, Weinheim